(Received 12 February 2025, Accepted 8 April 2025, Scheduled 3 May 2025)

SIW-Based Compact Four-Port MIMO Antenna with Enhanced Isolation for Wireless Communications

Vudattu Jaya Prakash[1,*], Vutukuri Leela Satyanarayana[1], Neelaveni Ammal Murugan[2], Inakoti Ramesh Raja[3], Krishna Dharavathu[1], and Shaik Mahaboob Subani[1]

[1]*Department of Electronics and Communication Engineering*
Potti Sriramulu Chalavadi Mallikarjunarao College of Engineering and Technology, Vijayawada, Andhra Pradesh, India
[2]*Department of ECE, SRM Institute of Science and Technology, Kattankulathur-603203, Tamilnadu, India*
[3]*Department of Electronics and Communication Engineering, Aditya College of Engineering and Technology (A) Surampalem, Andhra Pradesh, India*

ABSTRACT: This paper presents a four-port quarter-mode substrate integrated waveguide (QMSIW) MIMO antenna designed for 2.1 GHz wireless applications. The antenna employs orthogonally positioned complementary square-split ring resonator slots to achieve substantial miniaturization. Additionally, the mutual coupling between antenna elements is effectively minimized by incorporating cross-shaped slots between them, enhancing overall performance. The proposed four-port MIMO antenna achieves high isolation of 40 dB and features a compact electrical size of $0.19\lambda_0 \times 0.19\lambda_0$. The antenna demonstrates outstanding MIMO performance, with simulated and measured gains of 5.32 dBi and 5.44 dBi, respectively. Its efficiency is further supported by key performance metrics, including a low envelope correlation coefficient (ECC) of 0.0841 and a high diversity gain (DG) of 9.22 dB, ensuring enhanced signal reliability and reduced interference. With its compact structure, excellent isolation, and strong diversity performance, the proposed antenna serves as a highly suitable candidate for directional Wi-Fi applications.

1. INTRODUCTION

Multiple-Input Multiple-Output (MIMO) antennas are widely recognized for their ability to achieve high data rates, increased channel capacity, and improved spatial efficiency in communication systems [1, 2]. MIMO system performance is typically enhanced with a higher number of antenna elements, but this often comes at the cost of a larger physical footprint. While larger antennas can be spatially distributed to minimize mutual coupling between adjacent radiating elements, there is a growing demand for compact MIMO antenna designs that maintain low signal correlation among elements, especially for wireless applications [3]. Designing MIMO antennas presents a significant challenge in achieving compactness while ensuring high levels of isolation between channels. Substrate Integrated Waveguide (SIW) technology has emerged as a versatile and efficient platform for designing high-performance antennas [4, 5], offering advantages such as a high-quality factor, excellent power-handling capability, and low-loss performance [6–9]. These characteristics make SIW a preferred choice for applications requiring robust and reliable communication systems. Additionally, SIW inherently provides self-isolation between its guided modes, which is particularly beneficial for reducing the mutual coupling in multi-antenna systems such as MIMO. The flexibility of SIW technology enables the implementation of various cavity configurations, allowing designers to optimize antenna size and performance for specific applications. For instance, full-mode SIW (FMSIW) structures are often utilized in designs requiring maximum field confinement and power-handling capabilities. In contrast, half-mode SIW (HMSIW) [10, 11], quarter-mode SIW (QMSIW) [12, 13], and eighth-mode SIW (EMSIW) [14, 15] configurations offer compact solutions by utilizing only a fraction of the waveguide physical footprint without compromising performance. By leveraging these diverse configurations, MIMO antennas based on SIW technology have been developed to address the critical challenges of achieving compact size, high isolation, and superior performance. These designs cater to the growing demand for efficient and miniaturized antennas in advanced communication systems, making SIW an indispensable approach for next-generation wireless applications.

Several two-port SIW MIMO antennas have been developed using circular [16], rectangular [17], U-shaped [18], and tapered [19] slots, achieving a maximum isolation of > 30 dB. High isolation plays a vital role in MIMO systems, as it helps mitigate interference and significantly enhances overall performance. However, when four-port MIMO antennas are closely spaced, the mutual coupling between elements increases significantly, resulting in poor isolation. Increasing the spacing between elements can mitigate this issue but requires a larger footprint.

Multiple four-port MIMO antennas have been developed based on HMSIW, QMSIW, and EMSIW using semi-tapered slots [20], inverted L-shaped slots [21], T-shaped slots [22],

* Corresponding author: Vudattu Jaya Prakash (vjayaprakash0204@gmail.com).

self-isolated [23], Tai Chi-shaped slots [24], inverted U-shaped slots [25], and neutralizing lines [26].

In [27] and [28], four-port MIMO antennas were designed using mushroom-shaped slots and neutralized lines. These antennas occupy larger areas of $1.4\lambda_0 \times 1.4\lambda_0$ and $1.2\lambda_0 \times 1.2\lambda_0$, respectively. The neutralized lines provide a decoupling path to minimize current flow between elements, achieving enhanced isolation of $>$ 35 dB. A similar approach is followed in [26], where the four-port MIMO antenna achieves an isolation of >35 dB through the use of neutralized lines; however, the antenna occupies a larger electrical size of typically $\geq \lambda_0$ [16]. As the antenna size increases, the spacing between the elements increases, resulting in lower mutual coupling between them. On the other hand, four-port MIMO antennas have also been designed using T-shaped slots [25] and L-shaped slots [21], with these antennas occupying very small footprints of $0.61\lambda_0 \times 0.61\lambda_0$ and $0.58\lambda_0 \times 0.58\lambda_0$, respectively. Due to their small footprint, these antennas exhibit the high mutual coupling of 14 dB, since the antenna elements are positioned in close proximity. Similarly, an HMSIW-based MIMO antenna with semi-tapered slots [20] demonstrated improved isolation of 24 dB, but this was achieved with a relatively larger area of $0.77\lambda_0 \times 0.77\lambda_0$. These findings underscore the inherent trade-offs in MIMO antenna design, where compact sizes often compromise isolation, and higher isolation necessitates larger footprints. Addressing these challenges is critical to improving signal quality and data rates in modern wireless communication systems.

The four-port SIW-based MIMO antenna presented in this paper offers the following advantages: 1) high isolation of $>$ 40 dB, 2) compact size $0.19\lambda_0 \times 0.19\lambda_0$, and 3) a simple design structure. The results in this manuscript demonstrate the antenna's effectiveness for practical wireless applications.

2. DESIGN AND PERFORMANCE ANALYSIS OF A 4-PORT MIMO ANTENNA

Figure 1 illustrates the top and side views of the proposed 4-port MIMO antenna. The antenna is constructed with two copper layers, while the central dielectric substrate is composed of Rogers RT/Duroid 5870 material. The design parameters are optimized and given as: $L_{eff} = 28$, $a = 1$, $b = 1$, $c = 0.8$, and $d = 2$ (all the dimensions are in mm). Initially, an SIW square cavity resonator is designed, as shown in Fig. 2(a), with four 50 Ω microstrip feed lines. The fundamental resonant frequency of the SIW square cavity resonator in the TE_{mn0} mode [4] is obtained using 1

$$f_{mn0}^{SSCR} = \frac{c}{2\pi\sqrt{\varepsilon_r}}\sqrt{\left(\frac{m\pi}{l_{eff}}\right)^2 + \left(\frac{n\pi}{w_{eff}}\right)^2} \quad (1)$$

The effective length and width of the SIW Square Cavity Resonator (SSCR) can be determined based on the length (l_{eff}) and width (w_{eff}) of the top metallic plane. The via diameter and the distance between the vias are selected as $\frac{d}{\lambda_0} < 0.1$ and $s \leq \frac{d}{0.5}$ to avoid leakage losses from the SSCR [9]. The SIW cavity resonates at 5.01 GHz, which can be validated using Eq. (1). The reflection coefficients and the isolation of the SSCR are depicted in Fig. 2(b). To achieve miniaturization, a square complementary split-ring resonator (CSRR) slot is introduced in the SSCR. The dimensions of the slot are provided in Fig. 3(a). By loading the square-shaped CSRR slots (Antenna 1) with inner and outer side lengths of 10 mm and 12 mm, respectively, on all four sides of the top plane of the Square Cavity Resonator (SCR), the antenna achieves miniaturization.

The square-shaped CSRR slots increase the effective current path length within the cavity, resulting in a red shift of the operating frequency. The antenna's resonant frequency shifts from 5.01 to 2.85 GHz, yielding a frequency reduction of 43.11%. Antenna 1 resonates at 2.85 GHz, and the reflection coefficient and isolation are shown in Fig. 2(b). As observed in Fig. 5(a), by exciting port 2, strong mutual coupling exists between the adjacent ports. To achieve further miniaturization of the antenna, a square-shaped CSRR slot (Antenna 2) is introduced on the top metallic plane, featuring inner and outer side lengths of 6 mm and 8 mm, respectively, as illustrated in Fig. 3(b).

This additional slot creates an extra resonant mode, effectively reducing the overall resonant frequency of the antenna. The square split-ring slot enhances electromagnetic field interactions within the cavity, increasing the effective electrical length without significantly increasing the physical size of the antenna. It can be observed from Fig. 2(b),

Antenna 2 resonates at 2.15 GHz, achieving a miniaturization of 57.09%, reducing the frequency from 5.01 GHz to 2.15 GHz. Fig. 5(b) displays the electric field distribution of Antenna 2, where poor isolation exists among the four adjacent ports of the antenna. To enhance the isolation among the four ports, cross-shaped slots are introduced as shown in Fig. 3(c). These lines effectively reduce mutual coupling by suppressing unwanted electromagnetic interactions between ports, ensuring strong isolation. The enhanced isolation is achieved through the modification of the electromagnetic field distribution. The cross-shaped slots introduce localized impedance discontinuities, which effectively suppress mutual coupling between adjacent ports by reducing the strength of coupled fields. Antenna 3 resonates at 2.1 GHz, as shown in Fig. 4. The minimum port isolation between any two ports is $>$ 40 dB. The electric fields in Antenna 3 are concentrated near the edges of square-shaped CSRR slots, a result of the resonant behavior of these

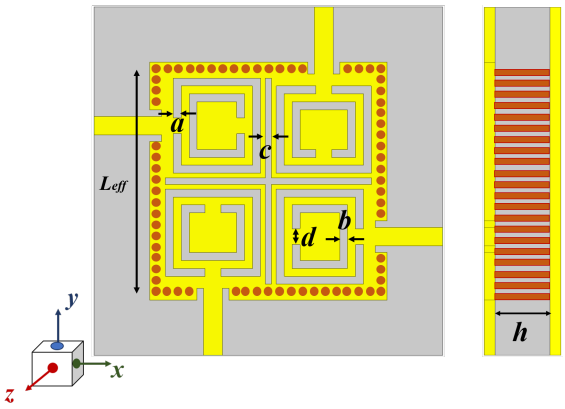

FIGURE 1. Schematic-view and lateral-view of the proposed MIMO antenna.

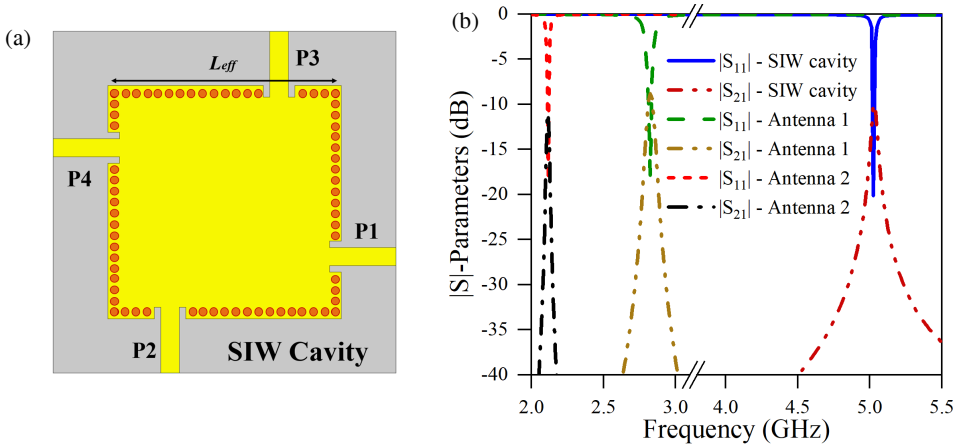

FIGURE 2. (a) SIW square cavity resonator, (b) $|S|$-Parameters of SIW cavity, Antenna 1, Antenna 2 and Antenna 3.

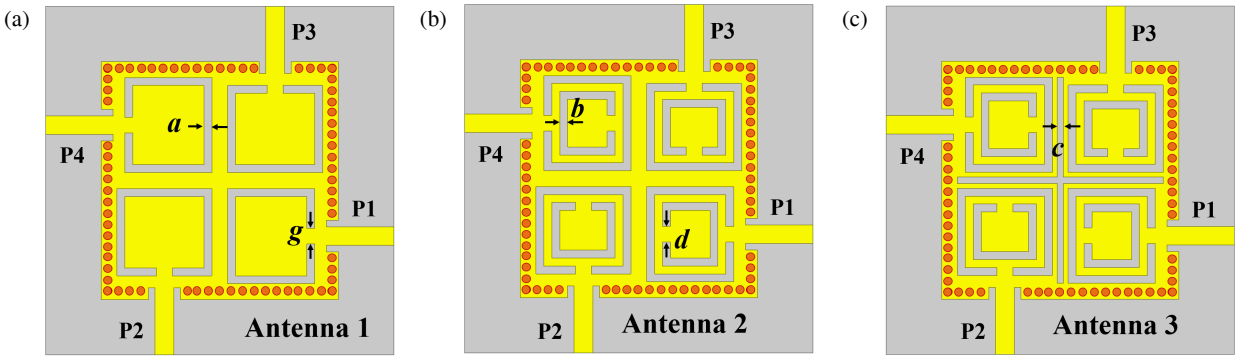

FIGURE 3. Design steps of the proposed MIMO antenna: (a) Antenna 1 with single CSRR-slots, (b) Antenna 2 with double CSRR-slots. (c) Antenna 3 with cross-shaped slots.

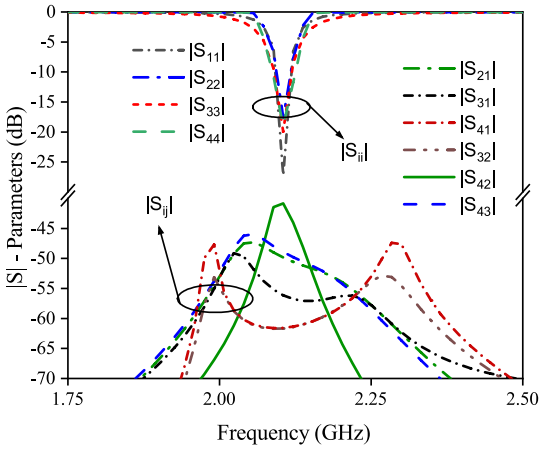

FIGURE 4. $|S|$-parameters of antenna 3.

slots. This design creates high-intensity electric fields along the slot boundaries, as the slots act as resonators that enhance the electromagnetic field in their immediate surroundings.

2.1. Analysis of MIMO Antenna Parameters

The antenna parameters are derived by changing the width of the outer square-shaped CSRR slot (a), the width of the inner square-shaped CSRR slot (b), the gap of the outer slot (c), and the gap of the inner slot (d). The effect of varying the width (a) from 0.5 to 1.5 mm on the resonant frequency is illustrated in Fig. 6(a). When the width a is less than 1 mm, there is no impedance matching. For values of a greater than 1 mm, significant interference exists among the elements. It can be observed from Fig. 6(b) that an optimized width of 1 mm is chosen, as it provides significant isolation and impedance matching between the antenna elements. Similarly, when parameter (b) is varied from 0.5 to 2 mm, an increase in b from 1 mm to 2 mm leads to higher mutual coupling between the antenna elements. For values of b less than 1 mm as shown in Fig. 6(c), there is no impedance matching. Thus, a width of 1 mm is chosen as the optimized value as shown in Fig. 6(d). In addition, varying the gaps in the inner and outer split-ring slots affects the inductance and capacitance between the elements, which in turn impacts isolation and impedance matching. After optimization, a gap of 2 mm is chosen for both the inner and outer slots. Fig. 7 depicts the steps involved in designing and optimizing the proposed antenna which are as follows:

- Choose an appropriate substrate material with minimal thickness to reduce losses and ensure low-profile structures. Use Eq. (1) to calculate the resonant frequency for the dominant TE_{110} mode of propagation in the SIW square cavity resonator.

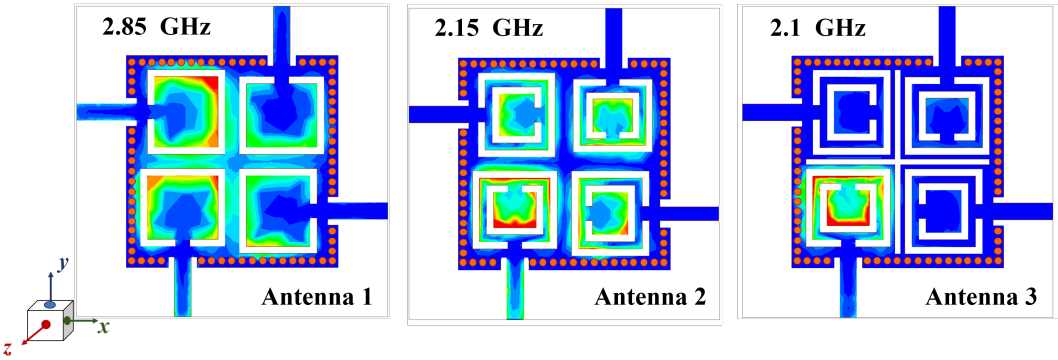

FIGURE 5. Electric field distributions of design steps (a) Antenna 1 operating at 2.85 GHz, (b) Antenna 2 operating at 2.15 GHz, (c) Antenna 3 operating at 2.1 GHz by the excitation of port 2.

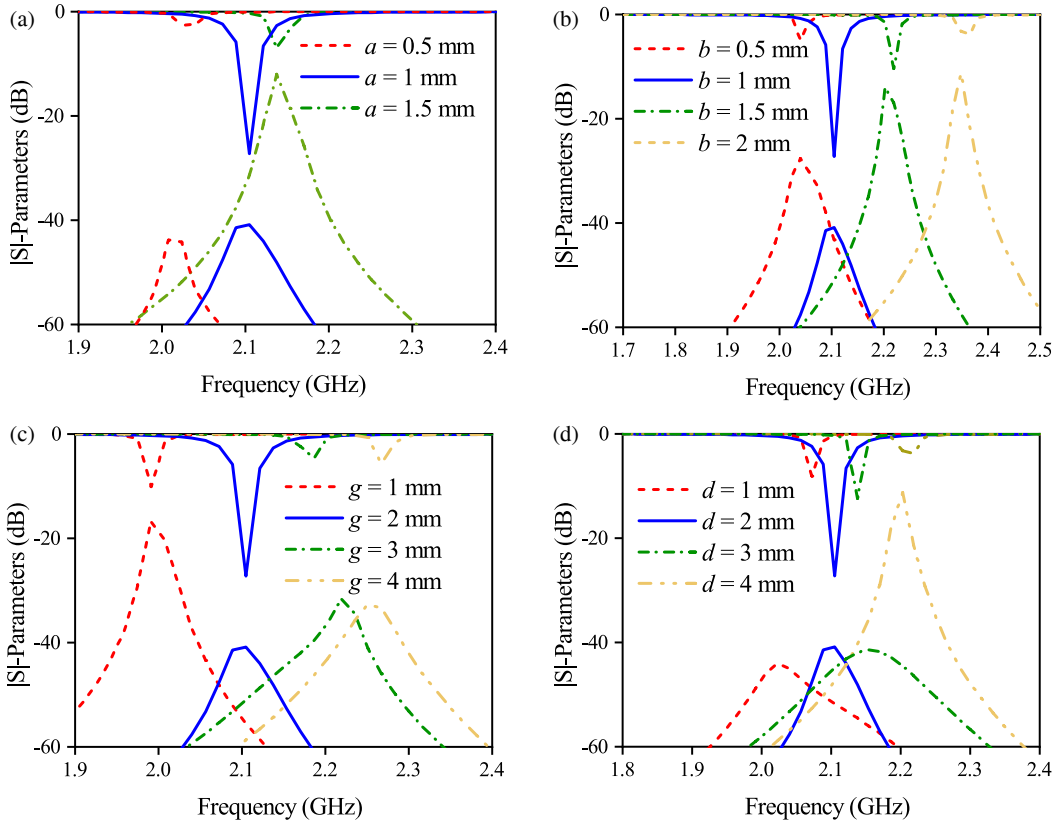

FIGURE 6. Optimized designed parameters of the proposed four port MIMO antenna.

- Calculate the effective length and width of the SIW square cavity resonator at operating frequency.
- Choose the via diameter and the spacing between the vias based on the conditions.
- Load a pair of CSRR slots on the QMSIW cavities and cross-shaped slots. The dimensions of the slots should be optimized by adjusting them according to the antenna's electrical wavelength, as discussed in the parametric analysis of the slots, to ensure that both isolation and miniaturization are achieved effectively.
- Check whether the desired parameters are achieved, and the antenna is ready for fabrication. Finally, validate the simulated and measured results.

3. RESULTS ANALYSIS AND DISCUSSION

Figure 8 shows the top view of the fabricated four-port MIMO antenna. Measurements of the reflection coefficients and isolation were carried out using a Keysight E5063A two-port vector network analyzer. The reflection coefficients were obtained by exciting port 1, operating at a frequency of 2.1 GHz, while isolation was measured between various port combinations: (1 and 2), (1 and 3), (1 and 4), (2 and 3), (2 and 4), and (3 and

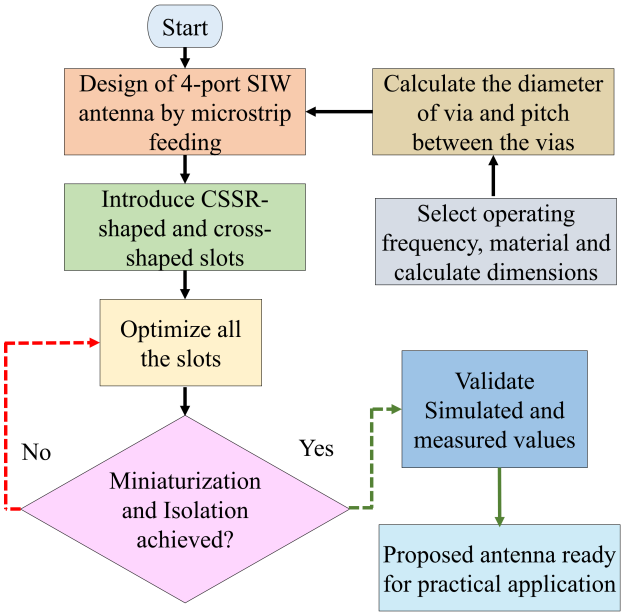

FIGURE 7. Design steps of the proposed MIMO antenna.

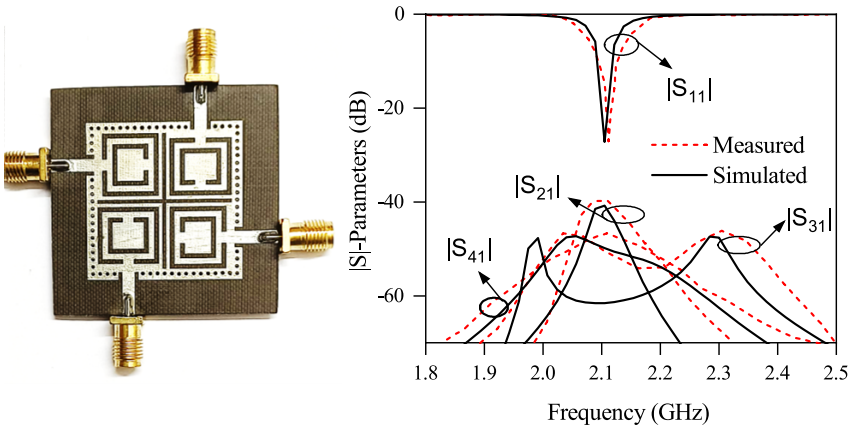

FIGURE 8. Photograph of the fabricated proposed MIMO antenna, and reflection coefficient and isolation simulated and measured values.

4). Fig. 8 also shows the simulated and measured isolations when port 1 is excited. The measured operating frequency of the MIMO antenna shows a discrepancy of less than 2% compared to the simulated resonant frequency. Furthermore, the overall isolation between any two ports (S_{21}, S_{31}, S_{41}, S_{23}, S_{24}, S_{34}) remains greater than 40 dB, as illustrated in Fig. 8.

The MIMO antenna design exhibits a directional radiation pattern, with peak radiation occurring in the broadside direction. Fig. 9 presents the normalized radiation patterns obtained from both simulated and measured values. The antenna exhibits a unidirectional radiation pattern, with the cross-polarization level surpassing 20 dB. The gain of the proposed MIMO antenna, based on simulations and measurements at 2.1 GHz, is recorded as 5.32 dBi and 5.44 dBi, respectively, as shown in Fig. 10. The antenna maintains a gain of $\geq$ 5 dB over a bandwidth of 2.04–2.13 GHz, indicating its ability to provide consistent radiation performance. Furthermore, the MIMO antenna demonstrates a radiation efficiency exceeding 80% when ports 1, 2, 3, and 4 are excited.

4. ANALYSIS AND PERFORMANCE OF DIVERSITY

The diversity performance of the 4-port MIMO antenna is assessed by examining parameters such as the mean effective gain, diversity gain, and envelope correlation coefficient. The ECC evaluates the correlation between the signals received by the antenna ports. To achieve effective diversity in radiation patterns, the ECC should ideally remain below 0.5 [29]. The ECC can also be calculated using the radiated far-field components by equation

$$\mathrm{ECC} = \frac{\left|\iint_0^{4\pi} \overline{E_1}(\theta,\phi)\cdot\overline{E_2}(\theta,\phi)\,d\Omega\right|^2}{\left(\iint_0^{4\pi}\left|\overline{E_1}(\theta,\phi)\right|^2 d\Omega\right)\left(\iint_0^{4\pi}\left|\overline{E_2}(\theta,\phi)\right|^2 d\Omega\right)} \quad (2)$$

The electric field distribution in the far-field region is represented as $E_1(\theta,\varphi)$ when Port 1 is excited, with Port 2 terminated using a matched load. Conversely, $E_2(\theta,\varphi)$ corresponds to the far-field electric field when Port 2 is excited, while Port 1 is matched. The ECC value is 0.007 computed based on

TABLE 1. Comparison of the performance of the proposed MIMO antenna with the existing SIW-based MIMO antennas.

Ref	Design Technique	Overall Size (λ_0^2)	Thickness (mm)	Frequency (GHz)	Isolation (dB)	Gain (dBi)
[27]	Neutralization lines	$1.4\lambda_0 \times 1.4\lambda_0$	1.57	4.5	35	6
[28]	Mushroom loading	$1.2\lambda_0 \times 1.2\lambda_0$	2.5	2.4	36	6.6
[26]	Neutralization lines	$1.08\lambda_0 \times 1.08\lambda_0$	1.5	5.025	36	5.6
[25]	T and anti-symmetric U-slots	$0.61\lambda_0 \times 0.61\lambda_0$	3	3.52	14	4.3
[21]	Back-to-back L-slots	$0.58\lambda_0 \times 0.58\lambda_0$	1.6	3.4	15	-1
[20]	Semi-taper slots	$0.77\lambda_0 \times 0.27\lambda_0$	3	4.83	24	8
[23]	Rectangular patch	$\lambda_0 \times 0.028\lambda_0$	1.57	4.43	35	6
TW *	**Square CSRR slots**	$\mathbf{0.19\lambda_0 \times 0.19\lambda_0}$	**0.787**	**2.1**	> 40	**5.32**

*TW indicates this work.

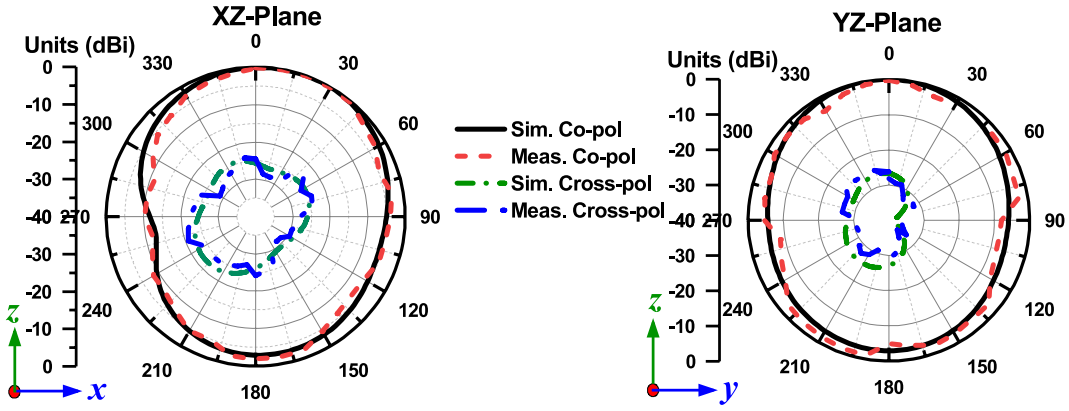

FIGURE 9. Normalized radiation pattern simulated and measured values in XZ and YZ planes.

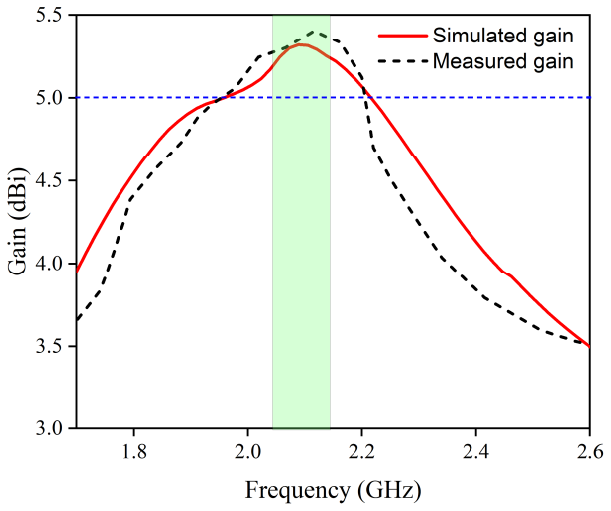

FIGURE 10. Simulated and measured gains of the proposed antenna.

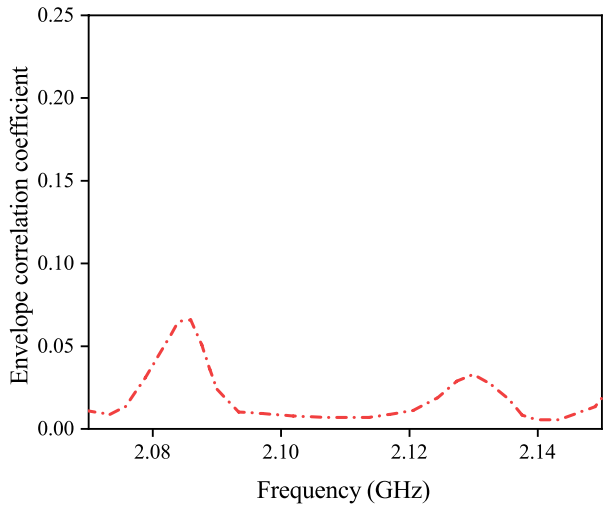

FIGURE 11. Analysis of the ECC of the proposed antenna.

these far-field characteristics, which is well within the acceptable range at 2.1 GHz, as shown in Fig. 11.

Additionally, the mean effective gain (MEG) is used to validate the performance of the proposed MIMO antenna. MEG represents the ratio of the average received power to the average incident power and is calculated using the S-parameters, as specified in 3.

$$MEG_i = 0.5\left[1 - \sum_{j=1}^{N} |S_{ij}|^2\right] \tag{3}$$

The MEG value is 0 dB, and its acceptable range is defined as $-12\,\text{dB} < \text{MEG} \leq 0$. For the proposed antenna, the simulated

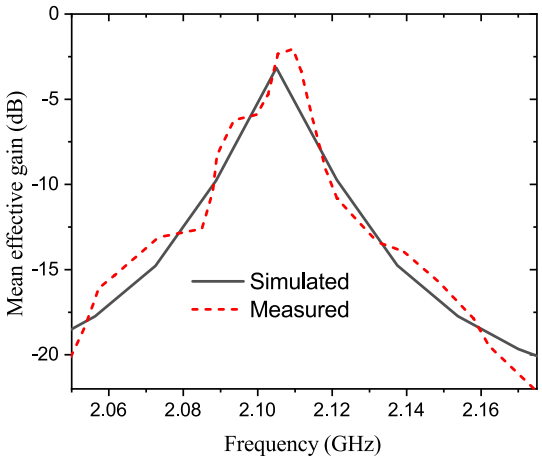

FIGURE 12. Mean effective gain of the proposed MIMO antenna.

MEG value is -3.16 dB, while the measured value is -2.34 dB, demonstrating excellent diversity performance, as illustrated in Fig. 12. Table 1 presents a comparison of the performance of the proposed MIMO antenna with other reported designs. In comparison, the antenna introduced in this work exceeds the performance metrics of other SIW-based MIMO antennas.

5. CONCLUSION

In this work, a four-port SIW MIMO antenna designed for 2.1 GHz wireless applications has been presented. The integration of square-shaped CSRR and cross-shaped slots in the antenna elements successfully achieved significant miniaturization and enhanced port isolation, with values exceeding 40 dB. The design process, including the strategic placement and dimension of the slots, is chosen to ensure optimal performance. The proposed antenna offers a compact footprint $0.19\lambda_0 \times 0.19\lambda_0$ and excellent diversity characteristics, validated through ECC, DG, and MEG metrics. These results establish the antenna as a promising solution for directional Wi-Fi applications, combining efficiency, compactness, and reliable performance for modern wireless systems.

REFERENCES

[1] Jensen, M. A. and J. W. Wallace, "A review of antennas and propagation for MIMO wireless communications," *IEEE Transactions on Antennas and Propagation*, Vol. 52, No. 11, 2810–2824, 2004.

[2] Rosaline, I., A. Kumar, P. Upadhyay, and A. H. Murshed, "Four element MIMO antenna systems with decoupling lines for high-speed 5G wireless data communication," *International Journal of Antennas and Propagation*, Vol. 2022, No. 1, 9078929, 2022.

[3] Gesbert, D., M. Kountouris, R. W. Heath, C.-B. Chae, and T. Salzer, "Shifting the MIMO paradigm," *IEEE Signal Processing Magazine*, Vol. 24, No. 5, 36–46, 2007.

[4] Wu, K., D. Deslandes, and Y. Cassivi, "The substrate integrated circuits-a new concept for high-frequency electronics and optoelectronics," in *6th International Conference on Telecommunications in Modern Satellite, Cable and Broadcasting Service, 2003. TELSIKS 2003.*, Vol. 1, P–III, Nis, Yugoslavia, Oct. 2003.

[5] Lokeshwar, B., D. Venkatasekhar, and A. Sudhakar, "Wideband low-profile SIW cavity-backed bilateral slots antenna for X-band application," *Progress In Electromagnetics Research M*, Vol. 97, 157–166, 2020.

[6] Bozzi, M., A. Georgiadis, and K. Wu, "Review of substrate-integrated waveguide circuits and antennas," *IET Microwaves, Antennas & Propagation*, Vol. 5, No. 8, 909–920, 2011.

[7] Deslandes, D. and K. Wu, "Single-substrate integration technique of planar circuits and waveguide filters," *IEEE Transactions on Microwave Theory and Techniques*, Vol. 51, No. 2, 593–596, 2003.

[8] Iqbal, A., I. B. Mabrouk, M. Al-Hasan, M. Nedil, and T. A. Denidni, "Wideband substrate integrated waveguide antenna for full-duplex systems," *IEEE Antennas and Wireless Propagation Letters*, Vol. 21, No. 1, 212–216, 2021.

[9] Deslandes, D. and K. Wu, "Accurate modeling, wave mechanisms, and design considerations of a substrate integrated waveguide," *IEEE Transactions on Microwave Theory and Techniques*, Vol. 54, No. 6, 2516–2526, 2006.

[10] Lai, Q., C. Fumeaux, W. Hong, and R. Vahldieck, "Characterization of the propagation properties of the half-mode substrate integrated waveguide," *IEEE Transactions on Microwave Theory and Techniques*, Vol. 57, No. 8, 1996–2004, 2009.

[11] Chaturvedi, D. and S. Raghavan, "Compact QMSIW based antennas for WLAN/WBAN applications," *Progress In Electromagnetics Research C*, Vol. 82, 145–153, 2018.

[12] Jin, C., R. Li, A. Alphones, and X. Bao, "Quarter-mode substrate integrated waveguide and its application to antennas design," *IEEE Transactions on Antennas and Propagation*, Vol. 61, No. 6, 2921–2928, 2013.

[13] Lokeshwar, B., J. Ravindranadh, and D. Madhavi, "Design and analysis of a bandwidth enhanced low-profile SIW cavity-backed slot antenna using TE_{210} mode," *Progress In Electromagnetics Research C.*, Vol. 125, 229–240, 2022.

[14] Luo, G. Q., Z. F. Hu, L. X. Dong, and L. L. Sun, "Planar slot antenna backed by substrate integrated waveguide cavity," *IEEE Antennas and Wireless Propagation Letters*, Vol. 7, 236–239, 2008.

[15] Gao, M., C. Liu, J. Nan, and H. Niu, "A broadband SIW cavity-backed circular arc-shaped slot antenna for millimeter-wave applications," *Progress In Electromagnetics Research Letters*, Vol. 117, 47–54, 2024.

[16] Nandi, S. and A. Mohan, "A compact eighth-mode circular SIW cavity-based MIMO antenna," *IEEE Antennas and Wireless Propagation Letters*, Vol. 20, No. 9, 1834–1838, 2021.

[17] Niu, B.-J. and J.-H. Tan, "Compact tri-band MIMO antenna based on quarter-mode slotted substrate-integrated-waveguide cavity," *International Journal of RF and Microwave Computer-Aided Engineering*, Vol. 30, No. 3, e22101, 2020.

[18] Niu, B. and J.-H. Tan, "SIW cavity MIMO antenna using hybrid boundaries and anti-symmetric U-shaped slots," *Progress In Electromagnetics Research Letters*, Vol. 86, 67–72, 2019.

[19] Wu, Y., K. Ding, B. Zhang, D. Wu, and J. Li, "SIW-tapered slot antenna for broadband MIMO applications," *IET Microwaves, Antennas & Propagation*, Vol. 12, No. 4, 612–616, 2018.

[20] Kumar Biswas, A. and U. Chakraborty, "Compact wearable MIMO antenna with improved port isolation for ultra-wideband applications," *IET Microwaves, Antennas & Propagation*, Vol. 13, No. 4, 498–504, 2019.

[21] Niu, B.-J. and Y.-J. Cao, "Bandwidth-enhanced four-antenna MIMO system based on SIW cavity," *Electronics Letters*, Vol. 56, No. 13, 643–645, 2020.

[22] Eslami, A., J. Nourinia, C. Ghobadi, and M. Shokri, "Four-element MIMO antenna for X-band applications," *International Journal of Microwave and Wireless Technologies*, Vol. 13, No. 8,

859–866, 2021.

[23] Elobied, A., X.-X. Yang, B. Du, and S. Gao, "Dual-polarized 2 × 2 MIMO antenna based on half mode substrate integrated waveguide," in *2019 13th European Conference on Antennas and Propagation (EuCAP)*, 1–3, Krakow, Poland, Mar. 2019.

[24] Shokri, M., C. Ghobadi, J. Nourinia, P. Pinho, Z. Amiri, R. Barzegari, A. Siahcheshm, F. Shapour, and K. Kaboutari, "A compact four elements self-isolated MIMO antenna for C-band applications," in *2023 IEEE 27th Workshop on Signal and Power Integrity (SPI)*, 1–4, Aveiro, Portugal, May 2023.

[25] Niu, B.-J. and J.-H. Tan, "Compact SIW cavity MIMO antenna with enhanced bandwidth and high isolation," *Electronics Letters*, Vol. 55, No. 11, 631–632, 2019.

[26] Elobied, A. A., X.-X. Yang, T. Lou, and S. Gao, "Compact 2 × 2 MIMO antenna with low mutual coupling based on half mode substrate integrated waveguide," *IEEE Transactions on Antennas and Propagation*, Vol. 69, No. 5, 2975–2980, 2020.

[27] Elobied, A. A., X.-X. Yang, N. Xie, and S. Gao, "Dual-band 2 × 2 MIMO antenna with compact size and high isolation based on half-mode SIW," *International Journal of Antennas and Propagation*, Vol. 2020, No. 1, 2965767, 2020.

[28] Zhai, G., Z. N. Chen, and X. Qing, "Mutual coupling reduction of a closely spaced four-element MIMO antenna system using discrete mushrooms," *IEEE Transactions on Microwave Theory and Techniques*, Vol. 64, No. 10, 3060–3067, 2016.

[29] Sharawi, M. S., A. T. Hassan, and M. U. Khan, "Correlation coefficient calculations for MIMO antenna systems: A comparative study," *International Journal of Microwave and Wireless Technologies*, Vol. 9, No. 10, 1991–2004, 2017.